(p,d) reaction on ^{62}Ni at 65 MeV

M. Matoba, K. Kurohmaru, O. Iwamoto, A. Nohtomi, Y. Uozumi, and T. Sakae
Department of Nuclear Engineering, Kyushu University, Fukuoka 812-81, Japan

N. Koori
Faculty of Integrated Arts and Sciences, The University of Tokushima, Tokushima 770, Japan

H. Ohgaki* and H. Ijiri
Graduate School of Engineering Sciences, Kyushu University, Kasuga 816, Japan

T. Maki and M. Nakano
School of Nursing and Technology, University of Occupational and Environmental Health, Kitakyushu 807, Japan

H. M. Sen Gupta
Department of Physics, the University of Dhaka, Dhaka-1000, Bangladesh
(Received 24 July 1995)

The ^{62}Ni$(p,d)^{61}$Ni reaction has been studied with 65 MeV polarized protons. Angular distributions of the differential cross section and analyzing power have been measured for neutron hole states in ^{61}Ni up to an excitation energy of 7 MeV. The data analysis with a standard distorted-wave Born approximation theory provides transferred angular momenta l and j and spectroscopic factors for several strongly excited states. The $1f_{7/2}$ hole state spreads largely in the excitation energy region of 2–6 MeV, while the $1f_{5/2}$, $2p_{3/2}$, and $2p_{1/2}$ hole states into only 2–4 levels. The strength function of the $1f_{7/2}$ hole state is analyzed with an asymmetrical Lorentzian function. The damping mechanism of the single hole states is discussed.

PACS number(s): 25.40.Hs, 21.10.Pc, 24.70.+s, 27.50.+e

I. INTRODUCTION

Recently, distributions of fragmented hole states have been found to be interesting for analyses of the spectral function of single hole stats in nuclei [1–3]. Asymmetrical Lorentzian and Gaussian forms have been applied in the analysis of the strength function. The Gaussian-type parametrization reproduced well the strength function of $1h_{11/2}$ and $1g_{7/2}$ neutron hole states in ^{207}Pb obtained by the ^{208}Pb (d,t) reaction at 200 MeV [4]. Spectral functions of the $1d_{5/2}$ neutron hole state obtained from one-nucleon pickup reactions [5,6] on ^{40}Ca were derived reasonably well by using the asymmetrical Lorentzian form, and compared with that of the corresponding proton hole state obtained from the $(d,^3\mathrm{He})$ and $(e,e'p)$ reactions [2]. More recently, the $1f_{7/2}$ neutron hole states in ^{59}Ni were also analyzed using the asymmetrical Lorentzian form [7].

As we can see in the cases of ^{40}Ca and ^{60}Ni(p,d) reactions [5–7], the strength of the $1d_{5/2}$ and $1f_{7/2}$ hole states splits into 20–30 levels, while that of single hole states near the Fermi surface into only 2–5 levels. This comes from that the spreading width of the hole state increases as a function of energy measured from the Fermi surface and the level density is, of course, low in the low excitation energy region. Since examples are scarce to discuss this problem in detail, it is desirable to investigate one-nucleon transfer reactions which excite single hole states. According to our previous works the angular distributions of cross section and analyzing power of the (p,d) reaction at 65 MeV can be used for clear assignment of the transferred angular momenta. And hence, the extracted spectroscopic factors should be reliable [5–8]. It is, therefore, interesting to restudy this type of reactions with a high resolution polarized beam and magnetic spectrograph system.

This paper describes results of a study on the ^{62}Ni(p,d) reaction measured with 65 MeV polarized protons. The measured energy spectra were analyzed in order to identify levels, to assign their spin parities, and to determine spectroscopic factors of the excited hole states in the excitation energy region of 0–6 MeV. The derived data are compared with the previous ones [9–13], in which those of a high resolution study by Koang *et al.* are important [11]. The fragmentation and spreading width of deeply bound $1f_{7/2}$ hole states in ^{61}Ni nucleus are discussed. The experimental pro-

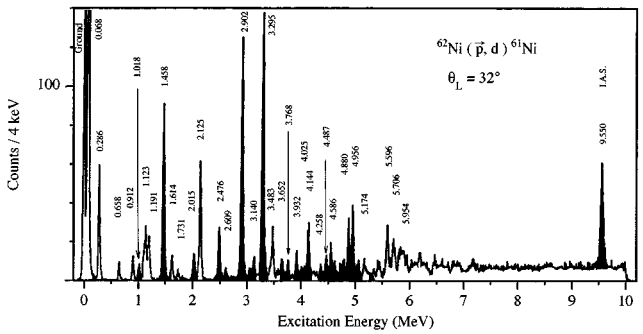

FIG. 1. Typical energy spectrum of deuterons from the ^{62}Ni $(p,d)^{61}$Ni reaction at 65 MeV.

*Present address: Electrotechnical Laboratory, Tsukuba, Japan.

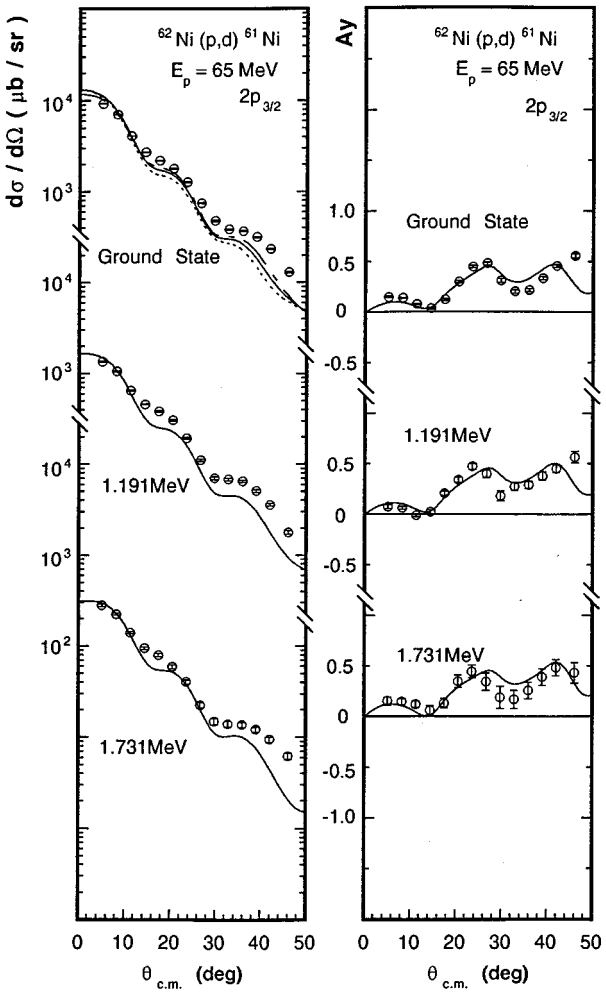

FIG. 2. Angular distribution data of cross sections (left) and analyzing powers (right) for $2p_{3/2}{}^{-1}$ transitions in the ^{62}Ni$(p,d)^{61}$Ni reaction at 65 MeV. The solid curves show predictions of the DWBA theory. The dotted curves are for bound-state parameters $r_n=1.31$ fm, and $a_n=0.62$ fm, and the dot-dash are for $r_n=1.19$ fm and $a_n=0.68$ fm.

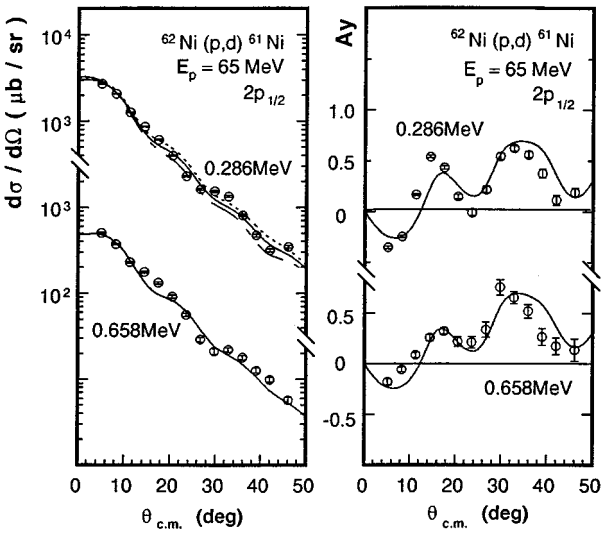

FIG. 3. Same as Fig. 2 for $2p_{1/2}{}^{-1}$ transitions.

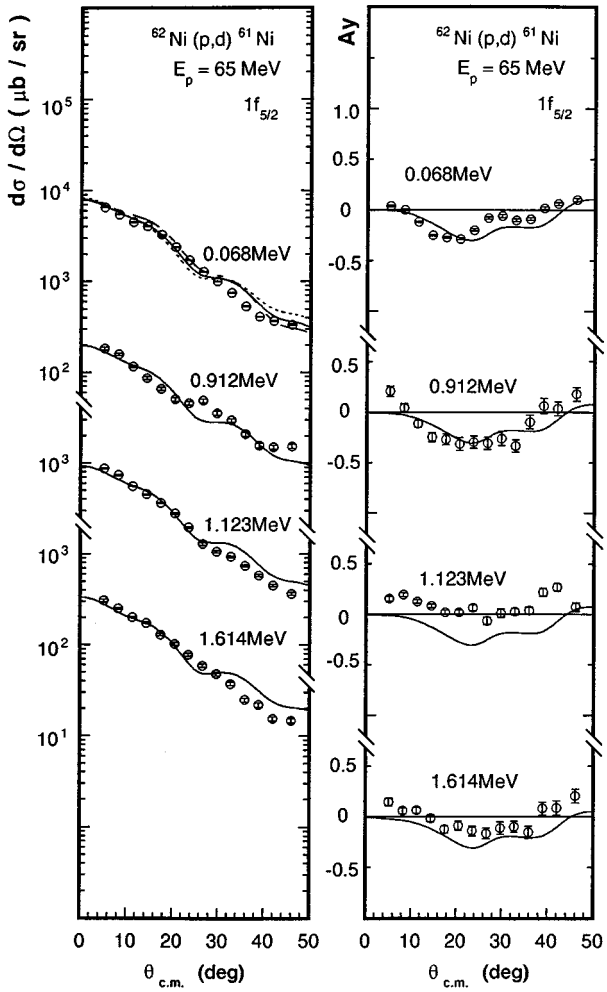

FIG. 4. Same as Fig. 2 for $1f_{5/2}{}^{-1}$ transitions.

cedure and results are presented in Sec. II, the theoretical analysis of angular distributions in Sec. III, and the assigned angular momenta and extracted spectroscopic factors in Sec. IV. The work is summarized in Sec. V. Preliminary results on the spreading width of the neutron hole states in ^{61}Ni were reported at a conference [14] and in a short note [15].

II. EXPERIMENT

A. Experimental procedure

The experiment was carried out at the AVF cyclotron facility of the Research Center for Nuclear Physics (RCNP), Osaka University. A polarized proton beam of 65 MeV energy was momentum analyzed and bombarded an enriched (99.7%) ^{62}Ni foil target of thickness 0.491 mg/cm^2. Emitted deuterons were detected in the focal plane of the spectrograph (RAIDEN) [16] viewed with the focal plane detector system KYUSHU [17]. Angular distributions of cross section and analyzing power were measured at 5°–45° (5–32° for higher excitation energy region) laboratory angles. The measured excitation energy region is 0–10 MeV. The normalization of the cross section is performed by scaling the measured $p+^{62}$Ni elastic scattering cross section to an optical model prediction using parameters of global potentials [18,19]. The accuracy of the normalization is esti-

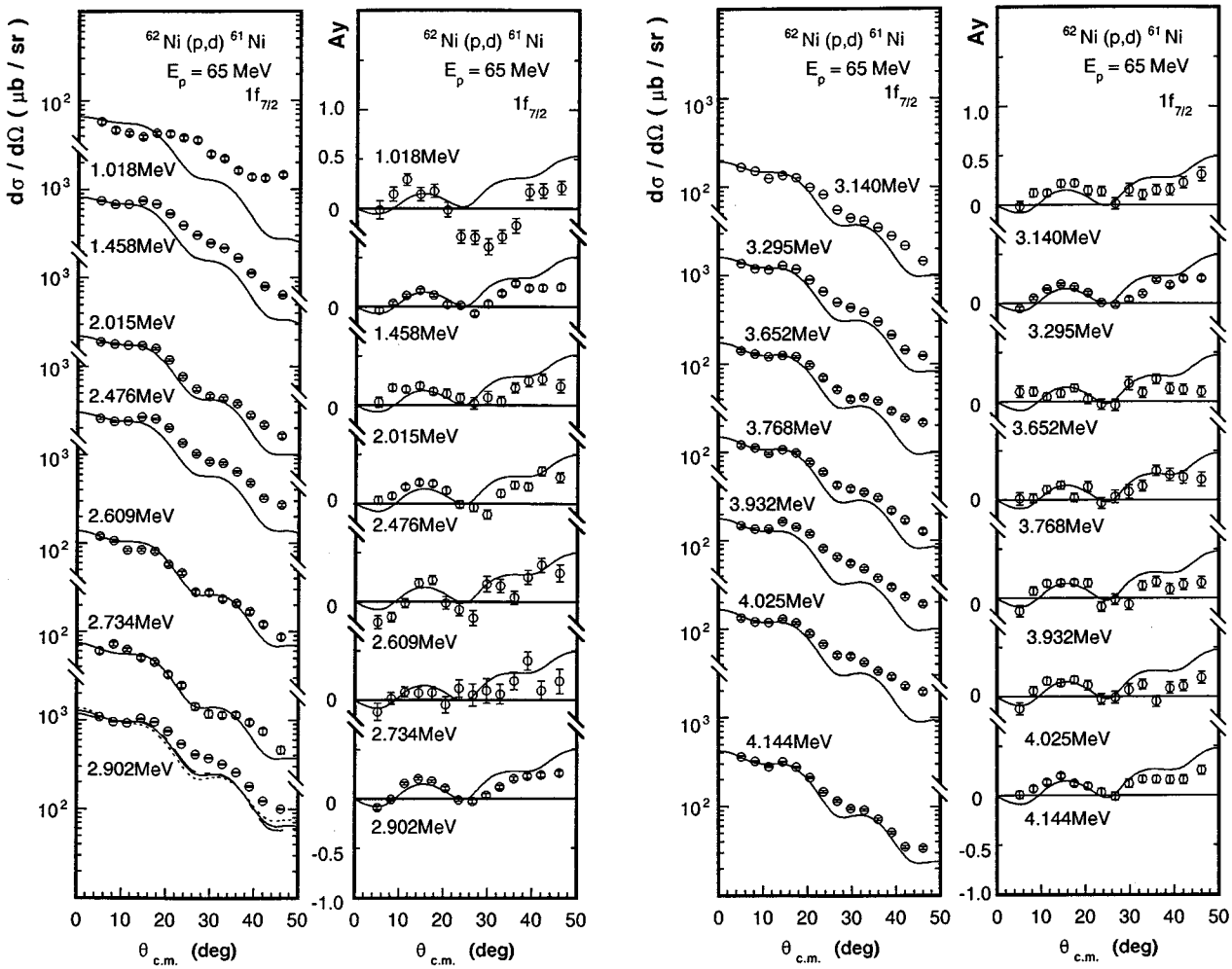

FIG. 5. Same as Fig. 2 for $1f_{7/2}{}^{-1}$ transitions.

mated to be better than 15%, which is mainly due to ambiguity of the procedure for fitting the theoretical to experimental angular distributions. The errors attributed to run-to-run variation to integrated beam current were of the order of a few %. The normalization factor so obtained has been checked with the values estimated from the standard target weight and solid angle measurements. The detail of the experimental method is described in our previous papers [5–8].

B. Experimental results

Figure 1 shows a typical deuteron energy spectrum from the ^{62}Ni(p,d) reaction in the excitation energy region of 0–10 MeV at 32° laboratory angle. The overall energy resolution was about 40 keV, which was due to effects of the beam energy width, the target energy loss, and the electronics noise in the position counter.

Discrete levels are distributed throughout the energy region up to the excitation energy of about 7 MeV. Some strongly excited states are found in the excitation energy region below 4 MeV and several strongly and weakly excited discrete states are distributed in the excitation energy region of 4–7 MeV.

The spectrum data were analyzed with a peak fitting and peeling-off program FOGRAS [20], which provided good data reduction for the complex peak spectra at the higher excitation energy region. Weak physical backgrounds were subtracted in the excitation energy region above 5 MeV. In the excitation energy region of higher than 6 MeV, groups of weakly excited state and a continuum plateau are found with a strongly excited state that is assigned to be isobaric analog state of the ground state of ^{61}Co. Peaks located at higher energies than 6 MeV were not analyzed because of ambiguity in the peak assignment. In previous works with lower bombarding energy projectiles, assignments of l and j values of some weakly excited states near $1\sim2$ MeV excitation energy were ambiguous in general. It is natural that the effects of coupling to collective states become weak as the bombarding energy increases and the momentum mismatching enlarges.

Angular distribution data for the analyzed states are shown in Figs. 2–9, together with the predictions of the distorted-wave Born approximation (DWBA) model as mentioned below. From the shapes of the angular distribution of cross section and analyzing power, the transferred l and j values are assigned definitely as is understood from the figures. The assignments are confirmed with the DWBA predictions.

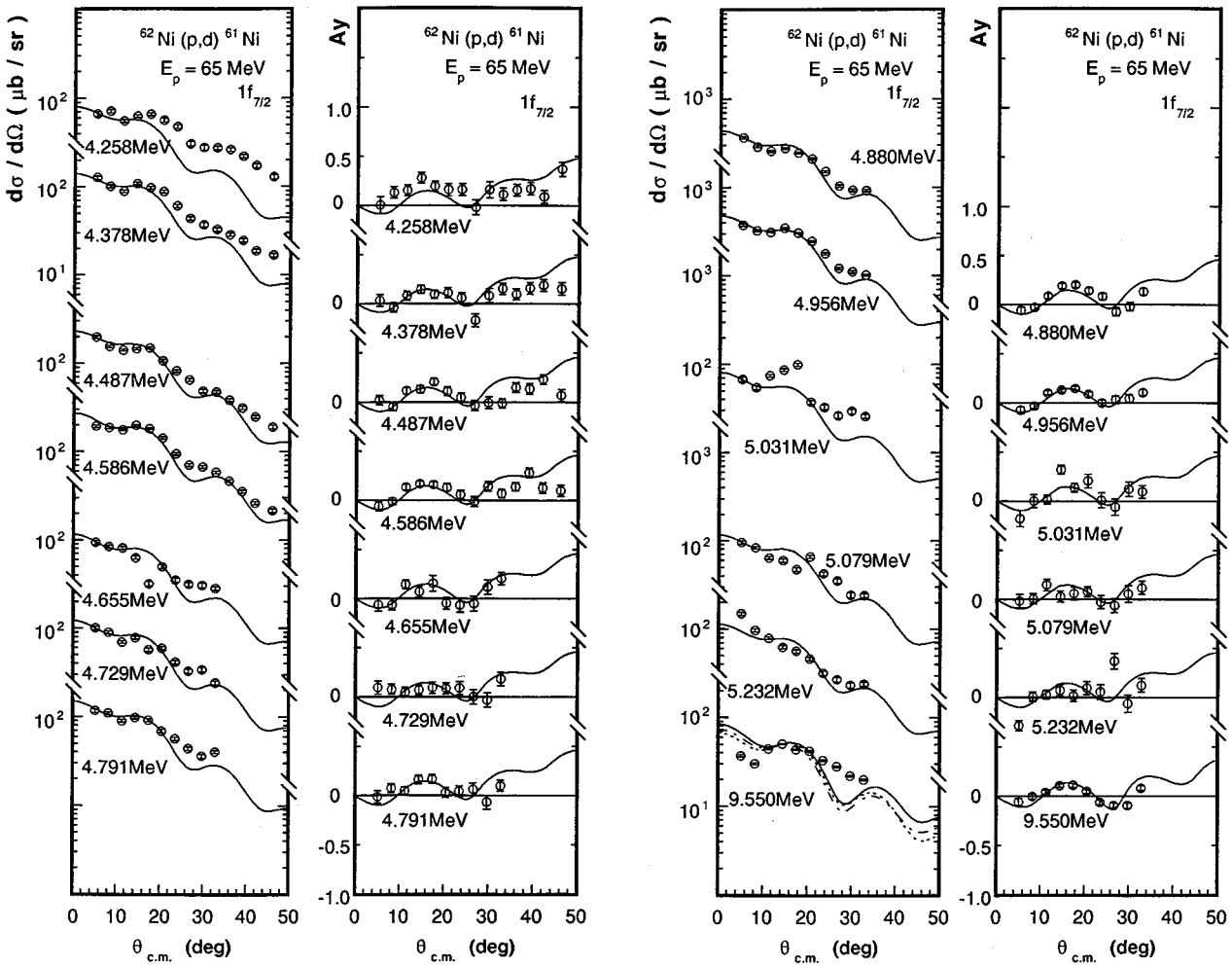

FIG. 5 (*Continued*).

Forty-nine peaks were analyzed in the excitation energy region below 6 MeV and the l and j values were assigned to 37 transitions. In some cases the assignments were tentative.

The angular distributions of the cross section and analyzing power for some transitions to very weakly excited states at the excitation energy of 0.9~1.5 MeV, show obscure oscillatory patterns as shown in Figs. 4 and 5. This may be an indication of the presence of higher order transfer reaction mechanism contributing to these states, for example, two-step processes via the collective 2^+ states of ^{60}Ni or ^{62}Ni nuclei.

The resultant assignments of l and j values for the excited states below 3 MeV are the same as those of Koang *et al.* [11] except for the 0.658 MeV state. The present j assignment of this state is $j=\frac{1}{2}$, which is also recorded in [13].

At the excitation energy higher than about 3 MeV, several excited states are also found in addition to strongly excited $1f_{7/2}$ hole states observed by Koang *et al.* The experimental results are summarized in Table I together with the results of Refs. [10,11].

III. DATA ANALYSIS

The differential cross section and analyzing power data were analyzed with the distorted-wave Born approximation (DWBA) code DWUCK [21] under the zero-range local energy approximation model. It is known that the conventional calculation with best-fit optical potentials in the proton and deuteron channels does not reproduce well the shape of differential cross-section data for (p,d) reactions at medium energies and the use of an adiabatic potential [22] for the deuteron channel improves considerably the overall fitting of the angular distribution. For protons, the global optical potential parameter of Menet *et al.* [18] and for deuterons, an adiabatic potential constructed with the proton and neutron optical potential parameters of Becchetti and Greenlees [19] were used. The optical potential parameter sets with definition of a standard form are listed in Table II.

The neutron bound-state wave functions were calculated in a standard Woods-Saxon well with the standard parameters $r_n=1.25$ fm and $a_n=0.65$ fm with a Thomas spin-orbit term with the usual $\lambda=25$ factor. The well depth was adjusted to yield the neutron separation energy with the effective binding energy method, because the usual separation energy method is known to be somewhat questionable for the analysis of states in a wide excitation energy region. The binding energies of the shell model orbits used in this paper are listed in Table III. These values are estimated from

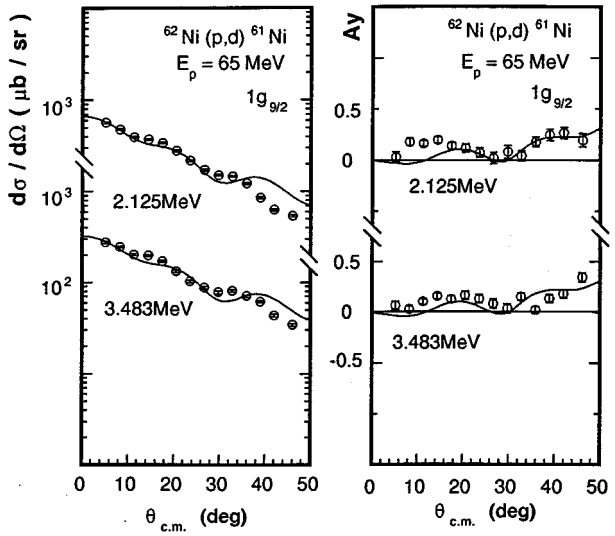

FIG. 6. Same as Fig. 2 for $1g_{9/2}{}^{-1}$ transitions.

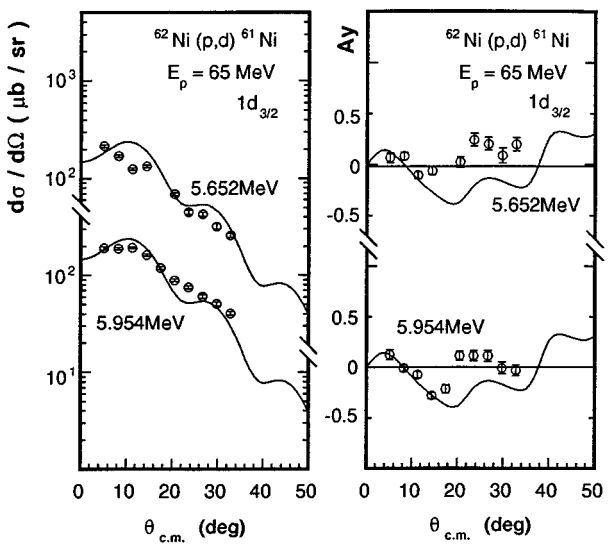

FIG. 8. Same as Fig. 2 for $1d_{3/2}{}^{-1}$ transitions.

(p,d) and (d,p) reaction data around ^{62}Ni nucleus [23,24] and present data.

In the local energy approximation model of DWBA, the parameter of the finite range effect 0.621 was used. And parameters of the nonlocality effect for neutron, proton, and deuteron potentials, $\beta_n = 0.85$, $\beta_p = 0.85$, and $\beta_d = 0.54$, respectively, were adopted. The spectroscopic factor for a (p,d) reaction for j transfer can be obtained using the equation

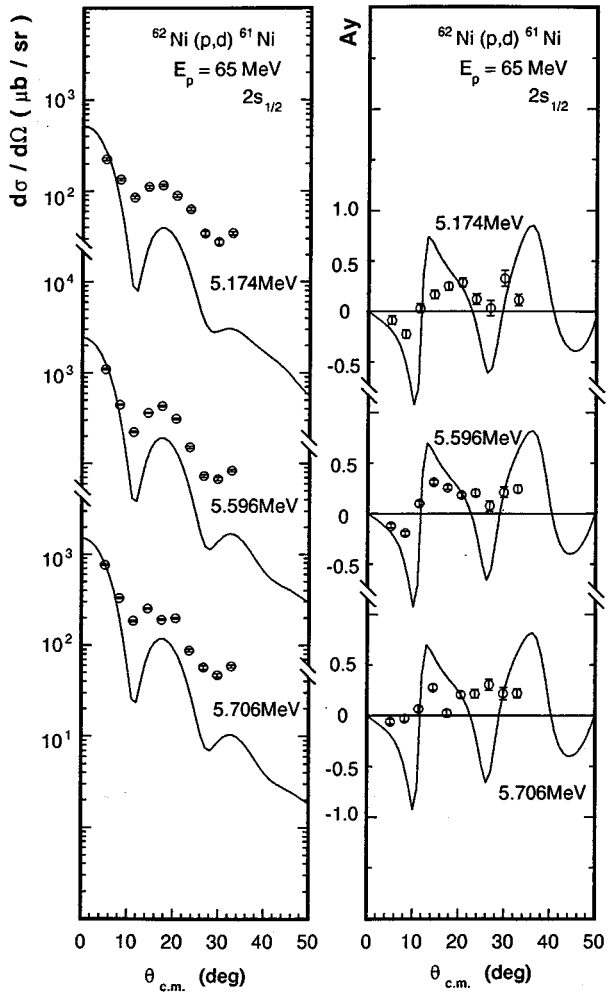

FIG. 7. Same as Fig. 2 for $2s_{1/2}{}^{-1}$ transitions.

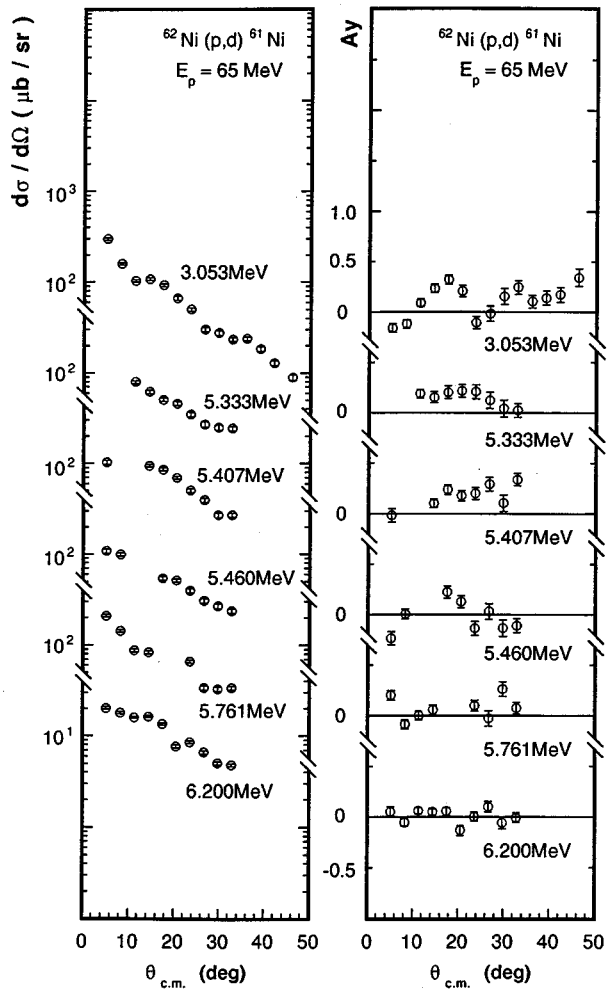

FIG. 9. Same as Fig. 2 for unassigned transitions.

TABLE I. Spectroscopic results from neutron pickup reactions on ^{62}Ni.

	This work (p,d)				Ref. [11] (p,d)				Ref. [10] $(^3\mathrm{He},\alpha)$			
No.	E_x (MeV)	l	J	C^2S	E_x (MeV)	l	J	C^2S	E_x (MeV)	l	J	C^2S
1	0	1	$\frac{3}{2}$	2.0	0	1	$\frac{3}{2}$	1.8	0	1	$\frac{3}{2}$	1.80
2	0.068	3	$\frac{5}{2}$	2.97	0.067	3	$\frac{5}{2}$	2.51	0.067	3	$\frac{5}{2}$	2.51
3	0.286	1	$\frac{1}{2}$	0.60	0.283	1	$\frac{1}{2}$	0.49	0.283	1	$\frac{1}{2}$	0.49
4	0.658	1	$\frac{1}{2}$	0.10	0.656	1	$\frac{3}{2}$	0.09				
5	0.912	3	$\frac{5}{2}$	0.081	0.909	3	$\frac{5}{2}$	0.09				
6	1.018	(3)	$(\frac{7}{2})$	(0.026)	1.020				1.020			
7	1.123	3	$\frac{5}{2}$	0.38	1.118	1,3	$\frac{1}{2},\frac{5}{2}$		1.118	1+3		
8	1.191	1	$\frac{3}{2}$	0.27	1.186	1	$\frac{3}{2}$	0.25	1.186	1	$\frac{3}{2}$	0.25
9	1.458	3	$\frac{7}{2}$	0.32	1.457	3	$\frac{7}{2}$	0.49	1.457	3	$\frac{7}{2}$	0.49
10	1.614	3	$\frac{5}{2}$	0.15	1.611	3	$\frac{5}{2}$	0.13	1.611	3	$\frac{5}{2}$	0.13
11	1.731	1	$\frac{3}{2}$	0.056	1.730	1	$\frac{1}{2},\frac{3}{2}$	0.06	1.730	1		
12	2.015	3	$\frac{7}{2}$	0.092	2.010	3	$(\frac{7}{2})$	0.09	2.010	3	$\frac{7}{2}$	0.09
13	2.125	4	$\frac{9}{2}$	0.22	2.120	(1,4)	$(\frac{9}{2},\frac{1}{2})$		2.120	1+4		
14	2.476	3	$\frac{7}{2}$	0.13	2.470	3	$\frac{7}{2}$	0.23	2.470	3	$\frac{7}{2}$	0.23
15	2.609	3	$\frac{7}{2}$	0.061								
16	2.734	(3)	$(\frac{7}{2})$	0.033								
17	2.902	3	$\frac{7}{2}$	0.57	2.899	3	$\frac{7}{2}$	0.80				
18	3.053				3.068	0	$\frac{1}{2}$	0.03				
19	3.140	3	$\frac{7}{2}$	0.086								
20	3.295	3	$\frac{7}{2}$	0.72	3.306	3	$\frac{7}{2}$	0.98	3.306	3	$\frac{7}{2}$	0.98
21	3.483	4	$\frac{9}{2}$	0.12								
22	3.652	3	$\frac{7}{2}$	0.083	3.657				3.657			
23	3.768	3	$\frac{7}{2}$	0.071								
24	3.932	3	$\frac{7}{2}$	0.084	3.939	3	$(\frac{7}{2})$	0.12				
25	4.025	3	$\frac{7}{2}$	0.078								
26	4.144	3	$\frac{7}{2}$	0.20								
27	4.258	3	$\frac{7}{2}$	0.038								
28	4.378	3	$\frac{7}{2}$	0.067								
29	4.487	3	$\frac{7}{2}$	0.11								
30	4.586	3	$\frac{7}{2}$	0.14	4.592	3	$(\frac{7}{2})$	0.18				
31	4.655	3	$\frac{7}{2}$	0.058								
32	4.729	3	$\frac{7}{2}$	0.061								
33	4.791	3	$\frac{7}{2}$	0.075								
34	4.880	3	$\frac{7}{2}$	0.23								
35	4.956	3	$\frac{7}{2}$	0.24	4.955	3	$\frac{7}{2}$	0.33				
36	5.031	(3)	$(\frac{7}{2})$	(0.041)								
37	5.079	3	$\frac{7}{2}$	0.059								
38	5.174	(0)	$(\frac{1}{2})$	(0.048)								
39	5.232	3	$\frac{7}{2}$	0.057								
40	5.333											
41	5.407											
42	5.460											
43	5.596	0	$\frac{1}{2}$	0.22	5.589	0	$\frac{1}{2}$	0.16				
44	5.652	(2)	$(\frac{3}{2})$	(0.20)								
45	5.706	0	$\frac{1}{2}$	0.14	5.697	0	$\frac{1}{2}$	0.12				
46	5.761											
47	5.954	2	$\frac{3}{2}$	0.20								
48	6.200											
49	9.550	3	$\frac{7}{2}$	0.37(I.A.S.)								

TABLE II. Optical model parameters used in the DWBA calculations for ^{62}Ni(p,d) ^{61}Ni reaction at 65 MeV.

Particle	V (MeV)	r (fm)	a (fm)	r_c (fm)	W_v (MeV)	W_s (MeV)	r' (fm)	a' (fm)	V_{so} (MeV)	r_{so} (fm)	a_{so} (fm)
Proton	40.98	1.16	0.75	1.25	7.05	2.45	1.37	0.32	6.04	1.06	0.78
Deuteron	[a]	1.17	0.78	1.25	[b]	[b]	1.29	0.61	4.13	1.06	0.75
Neutron	[c]	1.25	0.65						$\lambda=25$		

Nonlocality parameters		Finite-range parameter
p	0.85 fm	0.621
d	0.54 fm	

[a] $V=110.3-0.64(E_d/2)+0.4Z/A^{1/3}$ (MeV).
[b] $W_v=0.44(E_d/2)-4.26$ (MeV), $W_s=24.8-0.50(E_d/2)$ (MeV), E_d is the deuteron kinetic energy.
[c] Well depth adjusted to fit the separation energy.

$$\frac{d\sigma}{d\Omega}=2.30\frac{C^2S}{2j+1}\left.\frac{d\sigma}{d\Omega}\right|_{\text{DWUCK}}, \tag{1}$$

where C^2S is the spectroscopic factor for the transition and $d\sigma/d\Omega|_{\text{DWUCK}}$ is the resultant DWBA differential cross section with the code DWUCK [21]. The results of the DWBA analyses are shown in Figs. 2–8.

From comparisons between experiment and theory, the transferred angular momenta l and j were assigned, and then the spectroscopic factors were determined for 37 transitions in the excitation energy region from 0 to about 6 MeV. The results are summarized in Table I. For almost all the strongly excited states, the diffraction patterns are clear to assign the l and j values. The consideration of two-step process may be important to analyze some excited states which are excited from coupling with, for example, the surface vibration.

The extracted spectroscopic factors have errors of about $\pm 15\%$ due to the absolute cross-section normalization, as mentioned in Sec. II B. Additional errors should be considered on the uncertainty of the parameters for calculating the neutron bound state in DWBA analysis. In order to study the effect of a variation of the bound-state parameters on the shape and magnitude of the DWBA angular distributions, some strongly excited transitions were selected, which carry large C^2S values for $J^\pi=3/2^-$, $1/2^-$, $5/2^-$, $7/2^-$ (normal state) and $7/2^-$ (IAS). The geometrical parameters were changed by $\pm 5\%$ from the conventional values, i.e., $r_n=1.25$ fm and $a_n=0.65$ fm, with a constraint to keep the rms radius almost constant. Comparisons between the experimental and the DWBA angular distributions are made in Figs. 2–5 and the C^2S values are summarized in Table IV. As shown in the figures, angular distribution shapes do not depend so much on the choice of bound-state parameters, but the C^2S values depend quite appreciably. The uncertainty in the C^2S values becomes to be 20–30%. We then considered the adoption of the conventional bound-state parameters given in Table II.

A strongly excited $7/2^-$ state is found at 9.55 MeV excitation energy. This state is assigned as the isobaric analog of the ^{61}Co ground state [13,25] and the analysis with the DWBA theory should be done carefully. In the present work, however, further analysis with detailed reaction models has not been performed, because no other isobaric analog transitions are observed in the measured spectra. The extracted spectroscopic factor for this state is compared with the precious data and the estimated ones from the proton pickup reactions as described below.

IV. DISCUSSIONS

A. Single neutron hole states

The present results give information mainly on shell occupations in the $1f_{7/2}$, $2p_{3/2}$, $2p_{1/2}$, and $1f_{5/2}$ neutron hole orbits in ^{61}Ni, and also on those in deeper $1d_{3/2}$ and $2s_{1/2}$ hole orbits. It should be noted that the fragmentation of the hole strengths of valence orbits, $2p_{3/2}$, $2p_{1/2}$, and $1f_{5/2}$ is weak, and the number of transitions observed is only less than four. Contrary to this fact, the fragmentation of the $1f_{7/2}$ hole orbit is relatively large and the number of transitions is more than 20.

The number of the observed hole states for the $2p_{3/2}$, $2p_{1/2}$, and $1f_{5/2}$ orbits is almost the same as the results of four previous works [9–12], and no strengths corresponding to these orbits are found up to an excitation energy of about 6 MeV.

However, the number of states related to the $1f_{7/2}$ orbit becomes about twice of the previous results as shown in Table I. The present results are consistent with the fragmentation of the $1f_{7/2}$ hole states in the ^{59}Ni observed in the ^{60}Ni$(p,d)^{59}$Ni reaction at the excitation energies of 2.5–6 MeV [7,26]. This fact may correspond to the sudden spreading of the strength distribution above $E_x\sim 3$ MeV, as is understood from the strong correlation between the single hole state and the surface oscillation of the nucleus [27,28]. Also, the number of two-particle one-hole states which are able to couple to the single hole states increases rapidly in this energy region. The summed spectroscopic factors of the $2s_{1/2}$, $1d_{3/2}$, $1f_{7/2}$, $2p_{3/2}$, $2p_{1/2}$, and $1f_{5/2}$ orbits in the ^{61}Ni nucleus are shown in Table V together with previous results [10,11] and the simple shell model predictions. In a summation process of the spectroscopic factors, some data for which the assignment of transferred j values is ambiguous (cited in parentheses) are included, because of their weak effects on the final results.

TABLE III. Shell model binding energies used in the DWBA calculations for ^{62}Ni$(p,d)^{61}$Ni reaction at 65 MeV.

Orbit	E_n (MeV) [a]
$1g_{9/2}$	−8.995
$2p_{1/2}$	−9.887
$1f_{5/2}$	−10.371
$2p_{3/2}$	−10.794
$1f_{7/2}$	−14.020
$2s_{1/2}$	−16.179
$1d_{3/2}$	−16.552

[a]See text.

Although the absolute values of the spectroscopic factors have systematic errors arising, for example, from the optical model and bound-state parameters for DWBA analysis, it is important to compare results with the sum-rule limit because the data are always useful to discuss the quenching phenomena in the nuclear structure response.

The sums of the spectroscopic factors of neutron orbits for $T\pm\frac{1}{2}$ isospin states above a closed shell core are estimated with a simple shell model prescription as [29]

$$\Sigma C^2S = n_n - \frac{n_p}{2T+1} \quad \text{for} \quad T_< = T-\tfrac{1}{2}$$
$$= \frac{n_p}{2T+1} \quad \text{for} \quad T_> = T+\tfrac{1}{2}, \tag{2}$$

where n_n and n_p are the numbers of neutrons and protons, respectively, above the closed shell core and T is the target isospin. For the ^{62}Ni nucleus where the ^{40}Ca is thought to be a good closed shell core, i.e., $n_p=8$, $n_n=14$, and $T=3$, then the sum-rule limits of $\Sigma C^2S=6\frac{6}{7}$ $(1f_{7/2})$ $+6.0(2p_{3/2}+2p_{1/2}+1f_{5/2})=12\frac{6}{7}$ and $\Sigma C^2S=\frac{8}{7}$ $(1f_{7/2})$ for the $T=\frac{5}{2}$ and $\frac{7}{2}$ states, respectively, are predicted. The sum of the experimental values for $T_<$ component is 10.34 which is about 80.4% of the limit as shown in Table V, where the $1f_{7/2}$ hole strengths corresponding to the $T=\frac{7}{2}$ components are subtracted. The present result may become slightly larger if there is an additional possibility of fragmentation and missing of strengths in a higher excitation energy region. However, this value has considerable errors due to the uncertainty of the geometrical parameters for the neutron bound-state calculation in DWBA analysis and the errors of the absolute cross sections. Sums of the spectroscopic factors of $2p_{3/2}$, $2p_{1/2}$, and $1f_{5/2}$ hole orbits determined in this paper are almost similar to that of Koang *et al.* [11].

TABLE IV. Effect of bound-state parameters on the C^2S values.

			C^2S		
E_x (MeV)	J^π	r_n, a_n	1.25, 0.65	1.19, 0.68	1.31, 062
0.0	$\frac{3}{2}^-$		2.00	2.38	1.58
0.068	$\frac{5}{2}^-$		2.97	4.05	2.72
0.286	$\frac{1}{2}^-$		0.60	0.72	0.46
2.902	$\frac{7}{2}^-$		0.57	0.75	0.45
9.550	$\frac{7}{2}^-, T_>$		0.37	0.40	0.24

TABLE V. Summed spectroscopic factors for single hole states measured from neutron pickup reactions on ^{62}Ni.

Orbit	Experiment [a]	[b]	[c]	Simple shell model prediction
$2p_{1/2}$	0.70	0.49 (0.55)	0.49	
$1f_{5/2}$	3.58	2.73	2.64	6.0
$2p_{3/2}$	2.33	2.14 (2.20)	2.05	
$1f_{7/2}$	3.73	2.34 (2.73)	1.79	6.86$(T_<)$ [d]
Subtotal	10.34	7.7 (8.21)	6.97	12.86$(T_<)$
$2s_{1/2}$	0.41[e]	0.31		1.71$(T_<)$
$1d_{3/2}$	0.20[e]			3.43$(T_<)$

[a]Present work.
[b]Results of Koang *et al.* [11]. In parentheses, the states with ambiguous l and j.
[c]Results of Rundquist *et al.* [10].
[d]$T_<$ strengths only for the shells in which protons are fully occupied.
[e]Main strengths may distribute in higher excitation energy.

The spectroscopic factor for the 9.55 MeV isobaric analog state of ^{61}Co is 0.37, which is relatively smaller than the estimated value using Eq. (2) from the proton pickup reaction data, $C^2S_n=C^2S_p/(2T+1)=0.64$ [30]. The selection of bound-state parameters may remedy this difference [8].

It was mentioned earlier (Sec. III) that a detailed DWBA analysis of the angular distribution data of the ground-state analog was not attempted, as no other analog transition was observed. We only make a passing remark on the ground-state isobaric analog states as observed by us on other Ni isotopes [7,25,31].

In the ^{58,60}Ni$(p,d)^{57,59}$Ni reactions [25], a couple of weak peaks were observed on both sides of the main g.s. analog. These are clearly fragmented of the $7/2^-T_>$ states arising from the isospin mixing, which causes sharing of the strength to the IAS by neighboring $7/2^-T_<$ states. On the other hand, only a single level is observed in each of the ^{62,64}Ni$(p,d)^{61,63}$Ni reactions (present work and Refs. [25,33]) leading to the g.s. analog ($J^\pi=7/2^-$), but the line shape is clearly broadened. This is probably a consequence of the high level density in these nuclei (excitation energy being higher than in ^{57,59}Ni), so that the individual levels are not separately resolved.

The C^2S values for the g.s. analogs (present work and Refs. [7,31]) measured by our group are summarized in Table VI together with those from the ^{58}Ni(p,d) and ^{58,60,62}Ni(p,d) reactions studied by Polane *et al.* [32] and Sherr *et al.* [33], respectively. Since the latter two measurements were made with an energy resolution of about 100 keV, the two weak fragments of the g.s. analog in the ^{58}Ni$(p,d)^{57}$Ni reactions are not resolved. The C^2S values for all the Ni(p,d) reactions except for ^{58}Ni(p,d) reaction [31] were extracted by means of the usual bound-state geometry ($r_0=1.25$ fm and $a=0.65$ fm) including $\lambda=25$. The C^2S values quoted in the table for (p,d) reactions are based on the prescription of effective binding energy. The use of separation energy method gives $C^2S=1.45$, 0.67, and 0.70, instead of $C^2S=1.17$, 0.42, and 0.26 for ^{58}Ni, ^{60}Ni, and ^{62}Ni, respectively, that were estimated by Sherr *et al.* [33].

TABLE VI. Spectroscopic factors for the ground-state analog.

Reaction	E_x (MeV)	C^2S value (p,d)	$(d,^3\mathrm{He})$ $C^2S_p/(2T+1)$	Shell model* $n_p/(2T+1)$
^{58}Ni(p,d)	5.233	144,[a] 2.25,[e] 1.17 [f]	1.70,[g] 1.42,[h] 1.46,[i] 1.83[j]	2.67
^{60}Ni(p,d)	7.304	0.87,[b] 0.42[f]	0.76,[k] 1.26[j]	1.60
^{62}Ni(p,d)	9.550	0.37,[c] 0.26[f]	0.64[l]	1.14
^{64}Ni(p,d)	11.80	– [d]	0.50[m]	0.89

*The full $1f_{7/2}$, $T_>$ strength, assuming no fragmentation.
[a]Matoba *et al.* [31]. $r_n=1.27$ fm, $a_n=0.70$ fm are used for the bound-state calculation.
[b]Matoba *et al.* [7].
[c]Present work.
[d]No data are reported.
[e]Polane *et al.* [32].
[f]Sherr *et al.* [33].
[g]Reiner *et al.* [34].
[h]Marinov *et al.* [35].
[i]Wagner *et al.* [36].
[j]Mairle *et al.* [37].
[k]Mairle *et al.* [38].
[l]Marinov *et al.* [30].
[m]Seeger *et al.* [39].

Also included in the table for a comparison are the C^2S values predicted for the IAS's by the simple shell model as well as those expected from the $(d,^3\mathrm{He})$ reactions on these Ni isotopes [30,34–39].

No clear picture emerges from the comparison, as the C^2S_p values themselves have a large variation, except that the C^2S values obtained by our group (present work and Refs. [7,31]) are self-consistent and indeed they decrease systematically with increasing target T values, as shown also in Ref. [33].

Table VII shows the integrated properties of surface shell orbits. The spreading widths are calculated from the second moment of the energy difference from the average. The energies scaled from the Fermi surface are calculated with the prescription given in Ref. [8]. We used the values of spreading widths in order to estimate the imaginary parts of the bound state potential discussed in Refs. [2,40].

B. Strength function of the $1f_{7/2}$ neutron hole states

The strong fragmentation of the $1f_{7/2}$ neutron hole strength in ^{59}Ni is found by Nann *et al.* [26]. This fact has not been explained by an extensive shell model calculation using $1f_{7/2}$, $1f_{5/2}$, $2p_{1/2}$, and $2p_{3/2}$ neutron orbits. The strength distribution of the $1f_{7/2}$ hole orbits in ^{61}Ni is shown in Fig. 10. The present study on ^{61}Ni confirms the findings of Nann *et al.* in ^{59}Ni and shows the existence of a high energy tail up to 6 MeV as shown in the figure. This type of data is useful to discuss the shape and the sum-rule characteristics of the strength function for deeply bound hole states [7]. To analyze the strength function of the spectroscopic factor, these data are converted to C^2S values in the unit energy interval (MeV^{-1}) as shown in Fig. 11. Those for ^{59}Ni observed in the ^{60}Ni(p,d) reaction [7] are also shown. The energy interval is set to 0.5 MeV. The fragmentation of the $1f_{7/2}$ hole states in ^{59}Ni and ^{61}Ni is quite similar to each other. The distribution of the hole strength is predicted by using a modified Lorentzian function as follows [3,7]:

$$C^2S(E)=\Sigma C^2S(E)f(E),$$

$$f(E)=\frac{n_0}{2\pi}\frac{\Gamma(E)}{(E-E_F-E_R)^2+\Gamma^2(E)/4}, \tag{3}$$

and

$$\int_0^\infty f(E)dE=1,$$

where E_R is the resonance energy and n_0 is the renormalization constant (about one), which is due to the energy dependence of the spreading width and is exactly one if the spreading width $\Gamma(E)$ in Eq. (3) is constant. The spreading width is fairly well expressed with a function proposed by Brown and Rho [41] and Mahaux and Sartor [2] as

TABLE VII. Integral properties of spectroscopic factor, excitation energy and spreading width from the present results. ($E_x=0-6$ MeV).

Orbit	C^2S	$\bar{E}_x$ (MeV)	Γ (MeV)	$E-E_F$ (MeV)
$2p_{1/2}$	0.70	0.339	0.306	2.008
$1f_{5/2}$	3.58	0.264	1.040	1.933
$2p_{3/2}$	2.33	0.178	1.063	1.847
$1f_{7/2}$	3.73	3.543	2.514	5.212

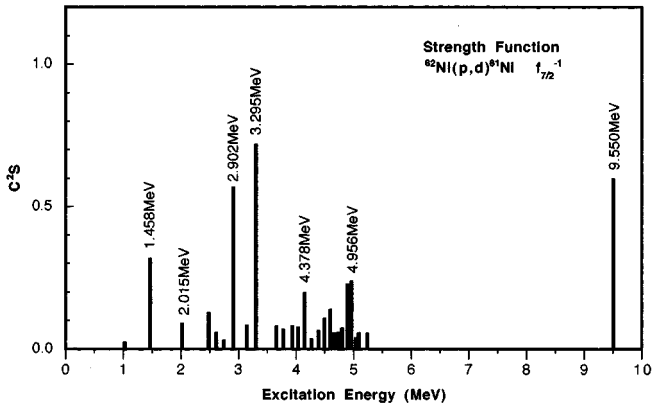

FIG. 10. Strength distribution of $1f_{7/2}{}^{-1}$ transitions from the ^{60}Ni(p,d)^{59}Ni reaction at 65 MeV.

$$\Gamma(E)=\frac{\varepsilon_0(E-E_F)^2}{(E-E_F)^2+{E_0}^2}+\frac{\varepsilon_1(E-E_F)^2}{(E-E_F)^2+{E_1}^2}, \qquad (4)$$

where ε_0, ε_1, E_0, and E_1 are constants that express effects of the nuclear damping in the nucleus. The first term in Eq. (4) corresponds just to the general trend of the infinite Fermi gas model prediction, with saturation characteristics in the $E\rightarrow\infty$ limit, and the second term to the existence of an additional onset of the nuclear damping near Fermi surface. The experimental data of spreading widths are well reproduced with Eq. (4) with the parameters determined as described in previous works [7,8,15]. The parameters $\varepsilon_0+\varepsilon_1$ were determined for the spreading width to approach to a constant value for the $E\rightarrow\infty$ limit, and ε_0 and E_0 to the infinite Fermi gas model prediction for the $E\rightarrow 0$ limit with the usual constant, $\varepsilon_0/{E_0}^2=17.5$ (MeV^{-1}) [7]. The $E\rightarrow\infty$ trend can be determined from the saturation property of the volume integral J_1 of the imaginary part of the optical potential [42,43]. In the present analysis an estimation by Brown and Rho, i.e., $J_1/A=130$ (MeV fm^3) was used [41]. The parameters of the second term ε_1 and E_1 were determined to fit the curve to the experimental data near a few MeV region.

The estimated parameters [7] are

$$\varepsilon_0=19.4\ \text{(MeV)},\quad E_0=18.4\ \text{(MeV)},$$

$$\varepsilon_1=1.40\ \text{(MeV)},\quad E_1=1.60\ \text{(MeV)}. \qquad (5)$$

Solid lines shown in Fig. 11 are the results for ^{59}Ni and ^{61}Ni calculated with Eq. (3) using the spreading width of Eq. (4) to keep the resonance energy E_R to the experimental and the total spectroscopic factor to the sum-rule limit for the $T_<$ component. The resonance energy E_R is estimated from the weighted mean of the distribution near peak region. The strength function is explained reasonable well by Eq. (3) using the energy dependence of the spreading width, Eq. (4). It should be noted that the curves for ^{59}Ni and ^{61}Ni are calculated with the same parameters, except for the resonance energy. To estimate this value, the spectroscopic factor above the $N=28$ closed shells, which is given from the difference 0.61 between the sum of the experimental spectroscopic factors, 6.61 and the shell model sum-rule limit

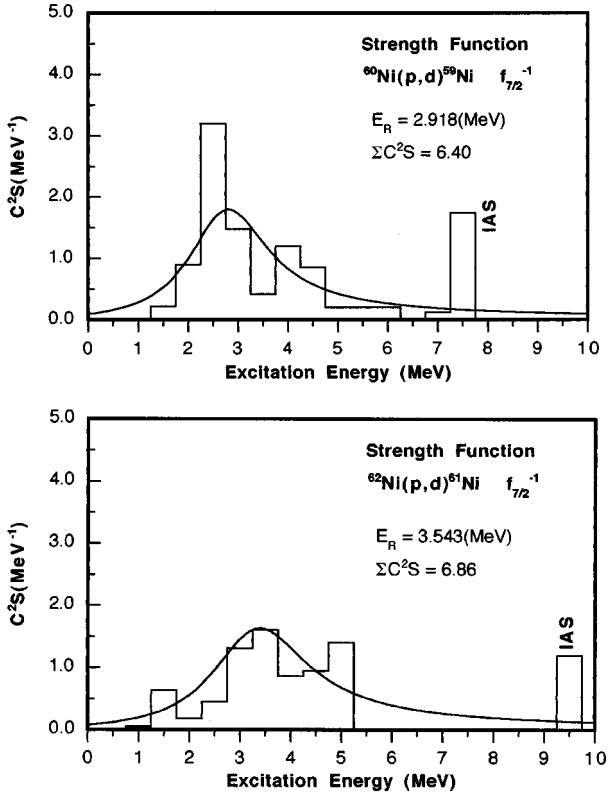

FIG. 11. Strength functions of $1f_{7/2}{}^{-1}$ transitions from the ^{60}Ni(p,d)^{59}Ni and ^{62}Ni(p,d)^{61}Ni reactions at 65 MeV, together with the prediction with a phenomenological model. See text.

$6(N=34-28)$ for $2p_{3/2}$, $2p_{1/2}$, and $1f_{5/2}$ hole transitions (Table V), is subtracted from the theoretical sum for the $1f_{7/2}$ hole state 6.86. Then, $3.73/(6.86-0.61)=59.7\pm 9.0\%$. The error is estimated from that of the fitting uncertainty of experimental and theoretical angular distributions mentioned in Sec. II. The theoretical estimation with Eqs. (3), (4), and (5), results in the existence of 66.3% strength in the observed energy region ($E_x<6.0$ MeV). Although the experimental strength is slightly smaller than the theory, the difference between the experiment and theory lies within the error.

If one considers the uncertainty of the absolute cross section and the parameters of bound-state wave function in DWBA analysis, this discrepancy may be understandable. It is important to increase the number of results from this type of analysis.

V. CONCLUSION

The ^{62}Ni(p,d)^{61}Ni reaction has been studied with 65 MeV polarized protons. The angular distributions of the differential cross section and analyzing power have been measured for single hole states in ^{61}Ni up to the excitation energy of 7 MeV.

The data analysis with a standard distorted-wave Born approximation theory provides transferred angular momenta l and j and spectroscopic factors for several

excited states. The strength function of the spectroscopic factors for the $1f_{7/2}$ hole state is analyzed with a modified Lorentzian function, and a reasonable fit is obtained. The higher energy tail in the strength function is analyzed in a consistent way with a model having one parameter, i.e., resonance energy with the parametrization of the spreading width [Eqs. (4) and (5)]. This analysis gives a new possibility to analyze the strength function of deeply bound hole states.

ACKNOWLEDGMENTS

We are grateful to the staff of the Research Center for Nuclear Physics (RCNP), Osaka University, for the support of the experiments at the cyclotron facility. This work was performed at the RCNP under Program Nos. 27A14 and 28A20. One of the authors (HMSG) acknowledges the financial support from the Ministry of Education, Science and Culture, Government of Japan, and the leave from the University of Dhaka.

[1] C. Mahaux and R. Sartor, Nucl. Phys. **A493**, 157 (1989).
[2] C. Mahaux and R. Sartor, Nucl. Phys. **A528**, 253 (1991).
[3] C. Mahaux and R. Sartor, Adv. Nucl. Phys. **20**, 1 (1991).
[4] H. Langevin-Joliot, J. van de Wiele, J. Guillot, E. Gerlic, L. H. Rosier, A. Willis, M. Morlet, G. Duhamel-Chretien, E. Tomasi-Gustafsson, N. Blasi, S. Micheletti, and S. Y. van der Werb, Phys. Rev. C **47**, 1571 (1993).
[5] M. Matoba, H. Ijiri, H. Ohgaki, S. Uehara, T. Fujiki, Y. Uozumi, H. Kugimiya, N. Koori, I. Kumabe, and M. Nakano, Phys. Rev. C **39**, 1658 (1989).
[6] M. Matoba, O. Iwamoto, Y. Uozumi, T. Sakae, N. Koori, T. Fujiki, H. Ohgaki, H. Ijiri, T. Maki, and M. Nakano, Phys. Rev. C **48**, 95 (1993).
[7] M. Matoba, O. Iwamoto, Y. Uozumi, T. Sakae, N. Koori, H. Ohgaki, H. Kugimiya, H. Ijiri, T. Maki, and M. Nakano, Nucl. Phys. **A581**, 21 (1995).
[8] K. Hisamochi, O. Iwamoto, A. Kisanuki, S. Budihardjo, S. Widodo, A. Nohtomi, Y. Uozumi, T. Sakae, M. Matoba, M. Nakano, T. Maki, S. Matsuki, and N. Koori, Nucl. Phys. **A564**, 227 (1993).
[9] R. H. Fulmer and W. W. Daehnick, Phys. Rev. **139**, B579 (1965).
[10] D. E. Rundquist, M. K. Brussel, and A. I. Yavin, Phys. Rev. **168**, 1296 (1968).
[11] D. H. Koang, W. S. Chien, and H. Rossner, Phys. Rev. C **13**, 1470 (1976).
[12] G. A. Huttlin, J. A. Aymar, J. A. Bieszk, S. Sen, and A. A. Rollefson, Nucl. Phys. **A263**, 445 (1976).
[13] Zhou Chunmei, Nucl. Data Sheet **67**, 271 (1992).
[14] M. Matoba *et al.*, in ''Contribution to 7th International Conference on Polarization Phenomena in Nuclear Physics,'' Paris, 1990, 45B.
[15] M. Matoba, T. Sakae, Y. Uozumi, O. Iwamoto, K. Hisamochi, H. Ijiri, Y. Watanabe, N. Koori, T. Maki, and M. Nakano, J. Phys. Soc. Jpn. **61**, 3827 (1992).
[16] H. Ikegami, S. Morinobu, I. Katayama, M. Fujiwara, and S. Yamabe, Nucl. Instrum. Methods **175**, 33 (1980).
[17] M. Matoba, K. Tsuji, K. Marubayashi, T. Shintake, H, Ikegami, T. Yamazaki, S. Morinobu, I. Katayama, M. Fujiwara, and Y. Fujita, Nucl. Instrum. Methods **180**, 419 (1981).
[18] J. J. H. Menet, E. E. Gross, J. J. Malanfy, and A. Zucker, Phys. Rev. C **4**, 1114 (1971).
[19] F. D. Becchetti, Jr. and G. W. Greenlees, Phys. Rev. **182**, 1190 (1969).
[20] S. Matsuki, code FOGRAS, Kyoto University, Chemical Research Institute (unpublished).
[21] P. D. Kunz, code DWUCK, University of Colorado (unpublished).
[22] R. C. Johnson and P. J. R. Soper, Phys. Rev. C **1**, 976 (1970).
[23] T. R. Anfinsen, K. Bjorndal, A. Graue, J. R. Lien, G. E. Sandvik, L. O. Tveita, K. Ytterstad, and E. R. Cosman, Nucl. Phys. **A157**, 561 (1970).
[24] G. A. Huttlin, S. Sen, W. A. Yoh, and A. A. Rollefson, Nucl. Phys. **A227**, 389 (1974).
[25] H. Ikegami, T. Yamazaki, S. Morinobu, I. Katayama, M. Fujiwara, Y. Fujita, H. Taketani, M. Adachi, T. Matsuzaki, N. Koori, and M. Matoba, Nulc. Phys. **A329**, 84 (1979) and references therein.
[26] H. Nann, D. W. Miller, W. W. Jacobs, D. W. Devins, W. P. Jones, and A. G. M. van Hees, Phys. Rev. C **28**, 642 (1983).
[27] P. F. Bortignon and R. A. Broglia, Nucl. Phys. **A371**, 405 (1981).
[28] G. F. Bertsch, P. F. Bortignon, and R. A. Broglia, Rev. Mod. Phys. **55**, 287 (1983).
[29] J. B. French and M. H. Macfarlane, Nucl. Phys. **26**, 168 (1961).
[30] A. Marinov, W. Oelert, S. Gopal, G. P. A. Berg, J. Bojowald, W. Hürlimann, I. Katayama, S. A. Martin, C. Mayer-Böricke, J. Meissburger, J. G. M. Römer, M. Rogge, J. L. Tain, P. Turek, L. Zemlo, R. B. M. Mooy, P. W. M. Glaudemans, S. Brant, V. Paar, M. Vouk, and V. Lopac, Nucl. Phys. **A431**, 317 (1984).
[31] M. Matoba *et al.* (unpublished).
[32] J. H. Polane, W. F. Feix, P. J. van Hall, S. S. Klein, G. J. Nijgh, O. J. Poppema, and S. D. Wassenaar, J. Phys. G **15**, 1715 (1989).
[33] R. Sherr, B. F. Bayman, E. Rost, M. E. Rickey, and C. G. Hoot, Phys. Rev. **139**, B1272 (1965).
[34] K. Reiner, P. Grabmayr, G. J. Wagner, S. M. Banks, B. G. Lay, V. C. Officer, G. G. Shute, B. M. Spicer, C. W. Glover, W. P. Jones, D. W. Miller, H. Nann, and E. J. Stephenson, Nucl. Phys. **A472**, 1 (1987).
[35] A. Marinov, W. Oelert, S. Gopal, B. Brinkmöller, G. Hlawatsch, C. Mayer-Böricke, J. Meissburger, D. Paul, M. Rogge, J. G. M. Römer, J. L. Tain, P. Turek, L. Zemlo, R. B. M. Mooy, P. W. M. Glaudemans, S. Brant, V. Paar, M. Vouk, and V. Lopac, Nucl. Phys. **A438**, 429 (1985).
[36] G. J. Wagner, A. Vdovin, P. Grabmayr, T. Kihm, G. Mairle, V. Pugatch, G. Seegert, and Ch. Stoyanov, Sov. J. Nucl. Phys. **40**, 887 (1984).
[37] G. Mairle, G. Th. Kaschl, H. Link, H. Mackh, U. Schmidt-Rohr, G. J. Wagner, and P. Turek, Nucl. Phys. **A134**, 180 (1969).

[38] G. Mairle, M. Seeger, M. Ermer, P. Grabmayr, A. Mondry, and G. J. Wagner, Nucl. Phys. **A543**, 558 (1992).
[39] M. Seeger, Th. Kihm, K. T. Knöpfle, G. Mairle, U. Schmidt-Rohr, J. Hebenstreit, D. Paul, and P. Von Rossen, Nucl. Phys. **A533**, 1 (1991).
[40] O. Iwamoto, A. Nohtomi, Y. Uozumi, T. Sakae, M. Matoba, M. Nakano, T. Maki, and N. Koori, Nucl. Phys. **A576**, 387 (1994).
[41] G. E. Brown and M. Rho, Nucl. Phys. **A372**, 397 (1981).
[42] C. Mahaux and H. Ngô, Phys. Lett. **100B**, 285 (1981).
[43] C. Mahaux and H. Ngô, Nucl. Phys. **A431**, 486 (1984).